A Heuristic Model for 3D Layered Materials with 2D Cationic Diffusion Currents from their Honeycomb Lattice

Godwill Mbiti Kanyolo[1] & Titus Masese[2,3]

[1]*Department of Engineering Science, The University of Electro-Communications 1-5-1 Chofu-gaoka, Chofu, Tokyo 182-8585, Japan*

[2]*Research Institute of Electrochemical Energy (RIECEN), National Institute of Advanced Industrial Science and Technology (AIST), 1-8-31 Midorigaoka, Ikeda, Osaka, 563-8577, Japan*

[3]*AIST-Kyoto University Chemical Energy Materials Open Innovation Laboratory (ChEM-OIL), Sakyo-ku, Kyoto 606-8501, Japan*

Honeycomb layered oxides are a novel class of materials generally exhibiting high ionic conductivity with battery applications. Owing to their honeycomb structure and layered framework, this class of materials is thought to harbor unique electrochemistry and physics. Here, a heuristic diffusion model of the charged alkali cations (such as lithium, sodium or potassium) in two-dimensional (2D) honeycomb layers within the three-dimensional (3D) crystal of honeycomb layered oxide is proposed. The model relates the excitation of cationic vacancies (by applied electromagnetic fields) to the Gaussian curvature deformation of the 2D surface. The quantum properties of the cations and their interlayer mixing through quantum tunneling are also considered. This work offers a novel theoretical framework for the study of 3D layered materials with 2D cationic diffusion currents, whilst providing pedagogical insights in the role of geometry in Brownian motion and quantum theory.

1 Introduction

Condensed matter physics is primarily concerned with studying the properties of all phases of matter *vis-a-vis* fundamental physics principles. Typically, this entails identifying an idealised, highly symmetric[a] or topologically constrained theoretical model which captures the physics of the relevant phenomena in question. In this regard, much of theoretical and experimental efforts mainly focus on highly symmetric crystal lattices with specific topologies where the bulk of the desirable physics occurs. Fairly recently, a burgeoning class of layered oxides with a honeycomb lattice (honeycomb layered oxides) has garnered interest due to a host of desirable electrochemical, magnetic and topological properties such as high voltage (high energy-density) capacity, magneto-spin interactions and high ionic conductivity.[1–16] These properties are attributed to their diversity of composition and the honeycomb lattice of the alkali charge carriers.

Here, we first introduce this diversity by classifying them in general formulae of the honeycomb layered compounds, whilst focusing on an exemplary sub-class adopting the composition $\mathrm{A}_2^+\mathrm{L}_2^{2+}\mathrm{D}^{6+}\mathrm{O}_6$ (or equivalently as $\mathrm{A}_{2/3}^+\mathrm{L}_{2/3}^{2+}\mathrm{D}_{1/3}^{6+}\mathrm{O}_2$), where $\mathrm{A} = \mathrm{K}, \mathrm{Li}$ or Na is an alkali cation (potassium, lithium or sodium respectively) constituting high ionic conductivity. Due to the large interslab/inter-layer separation distance ($\Delta z \gg l$ where l is the screening length of electromagnetic interactions along the z direction), the A cationic transport channels are typically confined to two dimensions (2D).

Secondly, we explore this cationic transport by considering a heuristic model of an idealised

[a] symmetries of the crystal, the action or quantum anomalies

three-dimensional (3D) layered material that we conjecture to capture the electrodynamics and diffusion properties of the cations in the honeycomb-layered materials described above. The idealised layered material admits diffusion currents along two dimensions (2D), where the inter-layers act as tunnel barriers classically untraversable by the cations. Finally, further insights are provided on possible effects of the honeycomb topology, applied magnetic fields and other crystalline symmetries expected to significantly impact the predictions of our heuristic model.

Throughout the paper, we set Planck's constant and the speed of light in the crystal to unity ($\hbar = \bar{c} = 1$.) We employ Einstein's summation convention together with the Minkwoski 2D + 1 and 3D + 1 metrics, $g_{ab} \equiv \mathrm{diag}(1, -1, -1)$ and $g_{\mu\nu} \equiv \mathrm{diag}(1, -1, -1, -1)$ to lower the Roman and Greek indices respectively. The Roman indices i, j, k are reserved for Euclidean space $g_{ij} \equiv \mathrm{diag}(1, 1, 1)$. We will apply minimal coupling procedure when considering curved spacetime.

2 Honeycomb Layered Oxides

Honeycomb layered oxides are a growing class of compounds, which generally adopt the following compositions:

$\mathrm{A_3^+L^{3+}D^{4+}O_5}(\mathrm{A^+_{6/5}L^{3+}_{2/5}D^{4+}_{2/5}O_2})$, $\mathrm{A_4^+L^{2+}D^{6+}O_6}$ ($\mathrm{A_8^+L_2^{2+}D_2^{6+}O_{12}}$ or $\mathrm{A^+_{4/3}L^{2+}_{1/3}D^{6+}_{1/3}O_2}$),

$\mathrm{A_2^+L^{3+}D^{5+}O_5}$ ($\mathrm{A^+_{4/5}L^{3+}_{2/5}D^{5+}_{2/5}O_2}$), $\mathrm{A_3^+L_2^{2+}D^{5+}O_6}(\mathrm{A^+L^{2+}_{2/3}D^{5+}_{1/3}O_2})$, $\mathrm{A_2^+L^{2+}D^{4+}O_6}$ ($\mathrm{A^+_{2/3}L^{2+}_{1/2}D^{4+}_{1/3}O_2}$),

$\mathrm{A_3^+A^{*+}L^{3+}D^{5+}O_6}$ ($\mathrm{A^+A^{*+}_{1/3}L^{3+}_{1/3}D^{5+}_{1/3}O_2}$), $\mathrm{A_2^+L_2^{2+}D^{6+}O_6}(\mathrm{A^+_{2/3}L^{2+}_{2/3}D^{6+}_{1/3}O_2})$, $\mathrm{A_2^+L_3^{2+}D^{4+}O_6}$

(or equivalently as $\mathrm{A^+_{2/3}L^{2+}D^{4+}_{1/3}O_2}$), $\mathrm{A_4^+L^{3+}D^{5+}O_6}(\mathrm{A_8^+L_2^{3+}D_2^{5+}O_{12}}$ or $\mathrm{A^+_{4/3}L^{3+}_{1/3}D^{5+}_{1/3}O_2}$),

$A_2^+D^{4+}O_3(A^+_{4/3}D^{4+}_{2/3}O_2)$, $A^+_{4.5}L^{3+}_{0.5}D^{6+}O_6$ $(A^+_{1/2}L^{3+}_{1/6}D^{6+}_{1/3}O_2)$, where L can be $Zn, Mn, Fe, Co, Cu, Ni, Cr, Mg$; D can be $Bi, Te, Sb, Ta, Ir, Nb, W, Sn, Ru, Mo$; A and A^* can be alkali atoms (such as Li, Cu, K, Rb, Cs, Ag and Na with $A \neq A^*$), transition metal atoms, for instance Cu or noble metal atoms (e.g., Ag, Au, Pd, etc). Over the years we have been witnessing a proliferation of various honeycomb layered compositions being reported.[1–11,17–38,40] From a crystal structural point of view, honeycomb layered oxides comprise alkali cations A^+ sandwiched in a framework containing layers or slabs of L and D atoms, coordinated octahedrally with oxygen atoms. The LO_6 and DO_6 octahedra assume a honeycomb configuration within the layers; thus the name – honeycomb layered oxides. **Figure 1** shows a honeycomb layered oxide framework with a general formula: $A_2^+L_2^{2+}Te^{6+}O_6$ $(A^+_{2/3}L^{2+}_{2/3}Te^{6+}_{1/3}O_2)$, where $A = Li, Na$ and K. We shall focus on this interesting oxide series due to its high ionic conductivity.[1,2,5–8] Indeed the manner in which the non-magnetic *A* cations are sandwiched between the magneto-active honeycomb layers of LO_6 and TeO_6 octahedra, endows the alkali A cations with very high diffusivity along the layers. Owing to their diversity of composition and high energy density, honeycomb layered oxides play host to rich electrochemistry that has found numerous applications especially in battery technology.[1–5,7,9,10,12,16,30,31,39]

In the next section, we shall explore generic properties such as the ionic transport along the 2D honeycomb channels by introducing a useful model from heuristic arguments.

3 The Model

We introduce a voltage, V producing an electric field $-\vec{\nabla}_{xy}V = (E_x, E_y, 0)$ in the x and y direction along the $x-y$ (honeycomb) plane of the crystal and preclude electromagnetic interactions and classical motion of A cations along the z direction (shown in **Figure 1**) which we assume are negligible due to the condition $\Delta z \gg l$, where Δz is the inter-layer/interslab separation and l is the screening length for electromagnetic interactions along the z direction.

Considering a single layer, and treating the cations as a fluid of charge density ρ, we can proceed to introduce the charge density vector $j^a = (\rho, \vec{j})$, where local charge conservation on the $x-y$ plane imposes the divergence condition $\partial_a j^a = 0$ with a solution, $j^a = \sigma_{xy}\varepsilon^{abc}\partial_b A_c$ where σ_{xy} is the conductivity of the cations in the $x-y$ plane, A_a is the electromagnetic vector potential and ε^{abc} is the totally anti-symmetric Levi-Civita symbol. This solution means that electromagnetic theory in 2D naturally leads us to the Chern-Simons term $\varepsilon^{abc}\partial_b A_c$.[41,42] This term contains only three electromagnetic fields: the magnetic field in the z direction, B_z and the electric fields, E_x and E_y in the x and y direction respectively, as displayed in **Figure 2(a)** & **2(b)**.

Ansatz 1 However, the honeycomb introduces further constraints on the electrodynamics of the cations. In particular, since the cations (absent the applied voltage) is known to form a 2D honeycomb lattice where the cations that contribute to the diffusion current (mobile cations) are assumed to be extracted by the potential energy of the applied voltage/electric fields (as shown in **Figure 2(b)**), the total number of these mobile cations ($g \in integer$) ought to be related (e.g. through **Figure 2(c)**) to the quasi-stable 2D configurations displayed in **Figure 2(d), 2(e)** & **2(f)**, where

each configuration supplies a unit mass m and charge q (where $q = +e \simeq 1.6 \times 10^{-19}$ C for $\mathrm{A} = \mathrm{K}, \mathrm{Na}, \mathrm{Li}$, *etc*) leaving a vacancy in the lattice while simultaneously constituting a diffusion current,

$$\vec{j} \equiv q\rho_{xy}(\vec{n} \times \vec{v}) = \sigma_{xy}(\vec{n} \times \vec{E}) \tag{1}$$

where $\vec{v} = (v_x, v_y, v_z)$ is the velocity vector, $\vec{E} = (E_x, E_y, E_z)$ is the applied electric field, $\vec{n} = (0, 0, 1)$ is the unit vector normal to the honeycomb surface oriented in the $x - y$ plane, $\rho_{xy} = -mK(x, y)/4\pi$ is their 2D mass density (equivalent to their 3D number density), $K(x, y)$ is the Gaussian curvature[43] of the honeycomb surface M after extraction of g cations which satisfies the definite integral (Gauss-Bonnet theorem[44]) $\int_M d(Area)K(x, y) = 2\pi\chi$ where $\chi = 2 - 2g$ is the Euler characteristic of the unbounded surface M with $g \in integer$ the genus of M. This means that $\int_M d(Area)\, \rho_{xy} \approx mg$ for $g \gg 1$ leading to $\int_M d(Vol)\, \rho_{xy} \equiv \int_M d(Area) \int_{1/m} dz\, \rho_{xy}(x, y) \approx g$.

Ansatz 2 We proceed by considering a second ansatz,

$$S(t, \vec{x}) = i \int dt\ \langle\psi|\frac{\partial}{\partial t}|\psi\rangle - \frac{i}{2}\int d\vec{x} \cdot \vec{n} \times D^{-1}\vec{v}, \tag{2a}$$

where $S(t, \vec{x})$ is the classical action, $|\psi\rangle$ is the quantum mechanical wavefunction (kernel) of the charged fluid of the cations respectively and D is the diffusion coefficient of the cations. Note that setting $d\vec{x}/dt = \vec{v}$, the kernel has the solution $|\psi\rangle = \exp(iS)$ as expected[b] (and thus satisfies the normalisation condition, $\langle\psi|\psi\rangle = 1$), since the second term becomes $\frac{1}{2}\int dt\, (d\vec{x}/dt) \cdot \vec{n} \times D^{-1}\vec{v} = \frac{1}{2}\int dt\, (dx^k/dt)D^{-1}\varepsilon_{ijk}n^i v^j = 0$ which identically vanishes.

For a closed path ∂M however, it need not vanish. In particular, plugging in eq. (1) into eq.

[b] by Feynman's path integral reformulation of quantum mechanics[45]

(2a) yields

$$\frac{1}{2}\oint_{\partial M} d\vec{x}\cdot\vec{n}\times\frac{\sigma_{xy}}{qD\rho_{xy}}\vec{E}=\frac{1}{2}\int_{M} d(Area)\,\vec{\nabla}_{xy}\cdot\frac{\sigma_{xy}}{qD\rho_{xy}}\vec{E}.$$

Substituting the Einstein-Smoluchowski relation $D=\mu\beta^{-1}$ and the Langevin result for ionic conductivity $\sigma_{xy}=q^2\mu\rho_{xy}$ yields by Stoke's theorem, $\frac{1}{2}q\beta\int_{\partial M}(E_y dx-E_x dy)=\frac{1}{2}q\beta\int_M d(Area)\vec{\nabla}_{xy}\cdot\vec{E}$. Naively, we are tempted to substitute Gauss' law of electromagnetism $\vec{\nabla}\cdot\vec{E}=q\rho_{xy}(x,y)/\epsilon$ to this result where ϵ is the permittivity within the 3D crystal. However, we ought to consider that the dynamics of the cations is confined in 2D where a Chern-Simons theory applies. This means that the 2D charge density is proportional to the flux[46] within the boundary ∂M shown in **Figure 2(b)**. Thus, instead we have $\vec{\nabla}_{xy}\cdot\vec{E}=-8\pi\rho_{xy}/q=2K(x,y)/q$ [c] and the argument of $|\psi\rangle$ transforms as $S\to S+i2\pi\beta m\Phi$ where we have defined the potential Φ as,

$$\int d(Area)\,K(x,y)\equiv-2\pi\Phi(x,y). \tag{2b}$$

Consequently, the solution for $|\psi\rangle$ transforms to,

$$|\psi\rangle=\exp i(S+i2\pi\beta m\Phi). \tag{2c}$$

This requires that $\Phi(x,y)\equiv-\frac{1}{4\pi}\int d\vec{x}\cdot\vec{n}\times\nu\vec{v}\to-\vec{\nabla}_{xy}\cdot\nu\vec{v}=2K(x,y)$ such that $1/\nu=m\mu=mD/k_{\mathrm{B}}T$ is the mean free time between collisions of the cations[d] where $\Phi(x,y)|_M=-\chi$.

[c] The factor of 8π is required for consistency with eq. (7)

[d] The definitions $\Phi(x,y)=-(4\pi m)^{-1}\int d\vec{x}\cdot\vec{n}\times\mu^{-1}\vec{v}$ and $\vec{\nabla}_{xy}\cdot\vec{E}=-8\pi\rho_{xy}/q$ are consistent with the Langevin equations $0=d\vec{p}/dt=-\mu^{-1}\vec{v}+q\vec{E}+\vec{\eta}$ and $0=d\vec{p}/dt=-\mu^{-1}\vec{n}\times\vec{v}+q\vec{n}\times\vec{E}+\vec{\eta}$ with the random force $\vec{\eta}=0$. See also eq. (4) and eq. (9c).

Notice that $\Phi(x,y)$ is reminiscent of a fictitious imaginary Aharonov-Casher phase[e] and $\int d(Vol)\psi^*\psi \equiv \langle\psi|\psi\rangle = \exp(-4\pi\beta m\Phi) \equiv \langle n\rangle$ takes the form of a Boltzmann factor[f] representing the dynamics of the cations. Setting $\psi = \langle\rho_{xy}\rangle^{1/2}\exp(iS)$ and $|\psi\rangle = \langle n\rangle^{1/2}\exp(iS)$ implies $\int d(Vol)\psi^*\psi = \int d(Vol)\langle\rho_{xy}\rangle = -\langle\chi\rangle/2 = \langle g\rangle - 1$ leading to the bosonic identity,

$$\langle g\rangle - \langle n\rangle = 1. \tag{3a}$$

In second quantisation formalism, the wavefunction can be defined as a Bogoliubov transformation,[47]

$$\hat{\psi} = \langle g\rangle^{1/2}\hat{a} + \langle n\rangle^{1/2}\exp(iS)\hat{a}^\dagger, \tag{3b}$$

$$\hat{\psi}^\dagger = \langle g\rangle^{1/2}\hat{a}^\dagger + \langle n\rangle^{1/2}\exp(-iS)\hat{a}, \tag{3c}$$

where $\hat{a}$ and $\hat{a}^\dagger$ are harmonic oscillator annihilation and creation operators respectively satisfying the commutation relation $[\hat{a},\hat{a}^\dagger] = [\psi,\psi^\dagger] = 1$ which is equivalent to eq. (3a). Thus, the wavefunction acts on the harmonic oscillator ground state as $\hat{a}\,|0\rangle = 0$ and $\langle 0|\,\hat{a}^\dagger = 0$ which guarantees $\hat{\psi}\,|0\rangle = |\psi\rangle$ and $\langle\psi| = \langle 0|\,\hat{\psi}^\dagger$. Finally, Boltzmann's entropy formula, $\mathcal{S} = \ln g$, where the genus $g \geq 1$ is taken as the number of microstates in the system, guarantees the entropy vanishes when $n = 0$ and the $g = 1$ torus given in **Figure 2(d)** represents the ground state of the system.

Typical diffusion dynamics in 3D We first note that for an Itō process driven by the standard Wiener process, the charge density function ρ of diffusive charges at equilibrium temperature sat-

[e] Aharonov-Casher phase $\gamma_{\rm AC} = -\int_{\partial M} d\vec{x}\cdot\vec{\mu}\times\vec{E}$ is the geometric phase acquired by the wavefunction of a neutral particle along a path ∂M around charges, where $\vec{\mu}$ is the magnetic moment of the neutral particle.[48,49]

[f] Alternatively, since the wavefunction is no longer normalised when $\Phi \neq 0$, it is clear that $\langle n\rangle \equiv \sqrt{Z}$ can also be interpreted as a Lehmann weight renormalising the wavefunction $|\psi\rangle \to |\Psi\rangle = \sqrt{Z^{-1}}\,|\psi\rangle$ and $\langle\Psi|\Psi\rangle = 1$.

isfy the Fokker-Planck equation,[50]

$$0 = \frac{\partial \rho}{\partial t} = -\vec{\nabla} \cdot \rho \vec{v} + \vec{\nabla} \cdot D \vec{\nabla} \rho,$$

equivalent to the Langevin equation

$$0 = m\frac{d\vec{v}}{dt} = -\frac{1}{\mu}\vec{v} + q\vec{\nabla}V, \tag{4}$$

and the Boltzmann factor $\rho \propto \exp -\beta q V$ which are typically used to derive $\sigma_{xy} = q^2 \mu \rho_{xy} = q\mu\rho$ and the Einstein-Smoluchowski relation $D/k_{\mathrm{B}}T = \mu$.

Diffusion dynamics of the cations in 2D However, as per **Ansatz 1**, $4\pi m\Phi \not\equiv qV$ is assumed to be directly linked to topology. Using our solution $\rho \propto \exp(-4\pi\beta m\Phi)$ where $\Phi = (-1/4\pi m)\int d\vec{x} \cdot \vec{n} \times \mu^{-1}\vec{v}$ is defined consistent with eq. (2a), we find that the appropriate Fokker-Planck equation at equilibrium for ρ is given by,

$$0 = \frac{\partial \rho}{\partial t} = -\vec{\nabla} \cdot (\vec{n} \times \rho \vec{v}) + \vec{\nabla} \cdot D \vec{\nabla} \rho. \tag{5a}$$

Together with the Chern-Simons current density $\vec{j} = \sigma_{xy}\varepsilon^{iab}\partial_a A_b$, the Fokker-Planck equation is solved by Fick's first law of diffusion,

$$\vec{j} = -D\vec{\nabla}\rho, \tag{5b}$$

to yield eq. (1).

The wavefunction in 2D + 1 dimensions It is necessary to establish the equation of motion for $|\psi\rangle = \exp i(S + i2\pi\beta m\Phi)$. In standard quantum mechanics, $|\psi\rangle$ simply satisfies the Schrodinger equation, $i\partial |\psi\rangle / \partial t = E_{\mathrm{a}} |\psi\rangle$ where $-\partial S/\partial t = E_{\mathrm{a}} \simeq m$ is the (activation) energy and mass

(equivalence relation) of a single cation. The presence of a finite screening length of electromagnetic interactions along the z direction presupposes that the inter-layer crystalline structures such as MO_6 and TeO_6 octahedra shown in **Figure 1** will act as tunnel barriers for the cations in the layers of the manifold M. This implies that, when $\Delta z \gg l \simeq 1/m$, the action (quantum phase) S satisfies the dynamics of a large tunnel junction,[51]

$$\partial_\mu S = \frac{q}{m} n^\nu F_{\mu\nu},$$

where $F_{\mu\nu} = \partial_\mu A_\nu - \partial_\nu A_\mu$ is the electromagnetic field tensor and $n^\mu = (0, \vec{n})$ is the unit normal four-vector along the z direction. Then, it is straightforward to show that $|\psi\rangle = \sqrt{N} \exp iS$ now obeys,

$$i\partial_\mu \ln |\psi\rangle = \frac{q}{m} n^\nu f_{\mu\nu} \rightarrow |\psi\rangle = \exp\left(-i\frac{q}{m}\int dx^\mu n^\nu f_{\mu\nu}\right), \tag{6}$$

where $S \rightarrow \ln|\psi\rangle$ and $F_{\mu\nu} \rightarrow f_{\mu\nu} = \partial_\mu A_\nu - \partial_\nu A_\mu + i\frac{\beta m}{2}\varepsilon_{\mu\nu}{}^{\sigma\rho}\partial_\sigma A_\rho$ is equivalent (in vector notation) to the Riemann-Silberstein[52] vector $\vec{F} = \vec{E} + i\frac{\beta m}{2}\vec{B}$ and is dual, $\vec{G} = \vec{B} + i\frac{\beta m}{2}\vec{E}$.[g]

Connection of the wavefunction, ψ to Gaussian Curvature In Riemannian geometry, the Gaussian curvature of a bounded 2D manifold M is given by, $K = \mathcal{R}/2$ where $\mathcal{R}$ is the Ricci scalar of the manifold M. Moreover, in **Ansatz 2**, we assumed $\vec{\nabla}_{xy} \cdot \vec{E} = -8\pi\rho_{xy}/q$, by assuming the proportionality (equivalence) of charge and flux in 2D.[46] Introducing a Hermitian tensor

[g] Strictly speaking, $f_{\mu\nu}$ is in the form of the (self-dual) Cabbibo-Ferrari tensor[53] given by $\partial_\mu A_\nu - \partial_\nu A_\mu + \varepsilon_{\mu\nu}{}^{\sigma\rho}\partial_\sigma a_\rho$, where $a_\mu = i\frac{\beta m}{2}A_\mu$ is the dual of the electromagnetic potential, A_μ. This self duality is taken as a consequence of the proportionality of flux and charge in 2D.

$K_{\mu\nu} = R_{\mu\nu} + iqF_{\mu\nu}$ defined on a $3\mathrm{D}+1$ Reimannian manifold,[h] we impose the condition,

$$\nabla^\nu K_{\nu\mu} = -\frac{8\pi}{m}\psi^*\partial_\mu\psi, \tag{7}$$

where $R_{\mu\nu}$ is the Ricci tensor, ∇_μ is the metric compatible covariant derivative and $\nabla_\sigma g_{\mu\nu} = 0$. Thus, this theory necessarily introduces a new field $g_{\mu\nu}$ (an emergent gravitational field[54]) describing the physics in the crystal.[i] This should not be entirely a surprise since the partition function is given by $N = \exp(-4\pi\beta m\Phi)$ and hence the free energy of the system $F = 4\pi m\Phi$ is proportional to a gravitational potential Φ.

Substituting $S = m\int dx^\mu U_\mu \equiv -m\int d\tau$ in $\psi = \sqrt{\rho_{xy}}\exp(iS)$ where U^μ is the four-velocity vector of the cations and using the Bianchi identity $\nabla^\nu R_{\mu\nu} = \partial_\mu R/2$, the real part and imaginary parts of eq. (7) become,

$$\partial_\mu R = -\frac{8\pi}{m}\partial_\mu\rho_{xy}, \tag{8a}$$

$$\nabla_\nu F^{\nu\mu} = -8\pi\rho_{xy}U^\mu/q, \tag{8b}$$

respectively. The solution for eq. (8a) is given by $\delta R \equiv R - 4\Lambda = -8\pi\rho_{xy}/m$, where R is the $3\mathrm{D}+1$ Ricci scalar and 4Λ is taken as the initial curvature of the manifold with no cations

[h] $K_{\mu\nu}$ is defined to satisfy $[D_\mu, D_\nu]U^\mu = K_{\mu\nu}U^\mu$ with $D_\mu = \nabla_\mu - iqA_\mu$ the covariant derivative and $U_\mu = \partial_\mu S$ the velocity four-vector.

[i] It is important to check the extent that $g_{\mu\nu}$ satisfies Einstein Field Equations.[55] Using eq. (9a), eq. (8a) and eq. (8b) together Bianchi identity, eq. (7) can be shown to transform to $R^{\mu\nu} - \frac{1}{2}Rg^{\mu\nu} + \Lambda g^{\mu\nu} = -\kappa T^{\mu\nu}$ with $T^{\mu\nu} = m\rho_{xy}U^\mu U^\nu + \epsilon_0(F^{\alpha\mu}F_\alpha{}^\nu - \frac{1}{4}F^{\alpha\beta}F_{\alpha\beta}g^{\mu\nu})$, $\kappa = 8\pi/m^2$ and $\epsilon_0 = \frac{q^2}{8\pi}$. In General Relativity, $\kappa = 8\pi G$ where G is the gravitational constant and ϵ_0 is the permittivity of free space. Comparing the two theories implies that our approach is equivalent to Einstein's gravitational theory with a charged particle of Planck mass $m = \sqrt{G^{-1}} = l^{-1}$ and Planck charge $q = \sqrt{8\pi\epsilon_0}$.

extracted from the $x-y$ plane by the electric field. Consequently, **Ansatz 1** requires that the curvature variation $\delta R \to \mathcal{R} = 2K$ reduces to the 2D Ricci scalar $\mathcal{R}$ under certain conditions satisfied by the honeycomb layered oxide. [j] Particularly, this limit entails introducing a time-like killing vector $\xi^\mu = (1, \vec{0})$ and a space-like Killing vector $n^\mu = (0, \vec{n})$, which impose the conditions $\xi^\mu \partial_\mu R = \partial R/\partial t = 0$ and $n^\mu \partial_\mu R = \partial R/\partial z = 0$ respectively.[k]

4 Significance

Electrodynamics of the cations. Notice that eq. (7) is invariant under the transformations $\partial_\mu \to \partial_\mu - iqb_\mu$ and $S = -m\int d\tau \to -m\int d\tau + q\int b_\mu U^\mu d\tau$ where b_μ is a gauge potential. The choice $b_\mu = \frac{1}{2}\int \epsilon_{\mu\nu}{}^{\sigma\rho}\partial_\sigma A_\rho dx^\nu$ with $\epsilon_{\mu\nu}{}^{\sigma\rho} \propto \varepsilon_{\mu\nu}{}^{\sigma\rho}$ the un-normalised Levi-Civita symbol (the normalisation factor to be determined) where $\epsilon^{0i\sigma\rho}\partial_\sigma A_\rho = \mathcal{B}_i$ and $\epsilon^{ij\sigma\rho}\partial_\sigma A_\rho = \varepsilon^{ijk}\mathcal{E}_k$ are the unnormalised magnetic and electric fields respectively, leads to equation of motion for the cations,[l]

$$mU^\nu \nabla_\nu U^\mu = qU_\nu \epsilon^{\nu\mu\sigma\rho}\partial_\sigma A_\rho. \tag{9a}$$

[j] Since $K(x,y)$ is independent of t and z, the limit $\delta\mathcal{R} \to 2K(x,y)$ requires the Ricci scalar R to also be independent of t and z.

[k] A Killing vector K^μ satisfies[56] $\nabla_\mu\nabla_\nu K^\mu = R_{\mu\nu}K^\mu$. Using the anti-symmetry relation $\nabla_\nu K_\mu = -\nabla_\mu K_\mu$ and the Bianchi identity $\nabla_\nu R^{\mu\nu} = \frac{1}{2}\nabla^\mu R$, the divergence $\nabla^\nu\nabla_\mu\nabla_\nu K^\mu = \nabla^\nu(R_{\mu\nu}K^\mu) = \frac{1}{2}K^\mu\nabla_\mu R$ identically vanishes.

[l] Deriving the equation of motion for the cations: $\partial_\mu S = mU_\mu + qb_\mu$ and $\nabla_\nu\partial_\mu S = m\nabla_\nu U_\mu + q\nabla_\nu b_\mu$. Using the fact that $\nabla_\nu\partial_\mu S = \nabla_\mu\partial_\nu S$ is symmetric, we find $m\nabla_\nu U_\mu - m\nabla_\mu U_\nu = q\nabla_\mu b_\nu - q\nabla_\nu b_\mu$. Contracting the expression with U^ν and using $U^\mu U_\mu = -1 \to \nabla_\nu(U^\mu U_\mu) = 2U^\mu\nabla_\nu U_\mu = 0$, we find $mU^\mu\nabla_\mu U^\nu = qU^\nu(\nabla_\mu b_\nu - \nabla_\nu b_\mu)$ equivalent to eq. (9a).

Recall, we introduced a t-like vector ξ^μ and z-like Killing vector n^μ to guarantee the independence of the Ricci scalar R on these coordinates. In the weak field limit[m] $\mathrm{diag}(g_{\mu\nu}) \simeq (1,-1,-1,-1) + small\,corrections$ with $U^\mu \simeq \exp(\Phi)(1,\vec{\mathcal{V}})$ and $U_\mu \simeq \exp(\Phi)(1,-\vec{\mathcal{V}})$ such that $U^\mu U_\mu = -1 \rightarrow U^0 = dt/d\tau = \exp(\Phi) = 1/\sqrt{1-\mathcal{V}^2} \rightarrow \Phi \geq 0$, eq. (9a) reduces to,

$$m\frac{dU^0}{dt} = q\vec{\mathcal{V}}\cdot\vec{\mathcal{B}}, \tag{9b}$$

$$m\frac{d(U^0\vec{\mathcal{V}})}{dt} = mU^0\vec{\nabla}g_{00}/2 + q\vec{\mathcal{B}} + q(\vec{\mathcal{V}}\times\vec{\mathcal{E}}), \tag{9c}$$

where g_{00} is the time-time component of the metric tensor related to $\xi^\mu = (1,\vec{0})$ by $g_{00} = \xi^\mu\xi_\mu$. Substituting eq. (9b) into eq. (9c) and identifying $\vec{\mathcal{V}} = \vec{n}\sqrt{1-\exp(-2\Phi)}$ as the velocity vector of the tunneling cations (pointing solely in the z direction) reduces eq. (9a) to,

$$-\frac{1}{2}\vec{n}\cdot\vec{\nabla}g_{00} \equiv \vec{n}\cdot\vec{\nabla}\Phi = 0, \tag{9d}$$

$$\frac{\partial}{\partial t}\Phi = \frac{q}{m}\vec{n}\cdot\vec{\mathcal{B}}\sqrt{\exp(2\Phi)-1} \equiv \frac{q}{4\pi m}\vec{n}\cdot\vec{B}, \tag{9e}$$

$$\vec{\nabla}\Phi \equiv -\frac{1}{2}\vec{\nabla}g_{00} = \frac{q}{m}\vec{n}\times\vec{\mathcal{E}}\sqrt{\exp(2\Phi)-1} \equiv \frac{q}{4\pi m}\vec{n}\times\vec{E}, \tag{9f}$$

where we have substituted $g_{00} = 1-2\Phi$ satisfying the weak field limit $0 \leq \Phi = (-1/4\pi\beta m)\int d\vec{x}\cdot\vec{n}\times\mu^{-1}\vec{v} \ll 1$, thus identifying Φ as the Newtonian potential and identified $4\pi\vec{\mathcal{B}}\sqrt{\exp(2\Phi)-1} = \vec{B}$ and $4\pi\vec{\mathcal{E}}\sqrt{\exp(2\Phi)-1} = \vec{E}$ as the magnetic field and the electric field as expected, thus fixing the normalisation factor for the Levi-Civita symbol to $\varepsilon^{\mu\nu\sigma\rho} = 4\pi\epsilon^{\mu\nu\sigma\rho}\sqrt{\exp(2\Phi)-1}$.

[m]The weak field limit entails taking the $small\,corrections$ to be related to the Newtonian potential. In particular, since $U^\mu\nabla_\mu U^\nu = dU^\nu/d\tau + \Gamma^\nu{}_{\sigma\rho}U^\sigma U^\rho$, where $\Gamma^\nu{}_{\sigma\rho} = g^{\mu\nu}(\partial_\sigma g_{\rho\mu} + \partial_\rho g_{\sigma\mu} - \partial_\mu g_{\sigma\rho})/2$ is the Christoffel symbol, in the weak field limit given by $\mathrm{diag}(g_{\mu\nu}) = (g_{00},1,1,1)$, the symbol is non-vanishing only for $\Gamma^i{}_{00} = -\vec{\nabla}g_{00}/2$.[57]

Equilibrium condition In the weak field static limit when the magnetic field vanishes as shown in **Figure 2(b)**, $\partial\Phi/\partial t = qB_z/m = 0$, eq. (8a) reduces,

$$\frac{1}{2}\nabla^2 g_{00} = -\frac{4\pi}{m}\rho_{xy}U^0U^0 \rightarrow \nabla^2_{xy}\Phi = -K\exp(2\Phi). \tag{10}$$

Equation (10) takes the form of the well-known Liouville's equation where $K = -4\pi\rho_{xy}/m$ is evidently the Gaussian curvature. For a constant conductivity, the charge density should vary spatially very slowly and an approximation can be made to solve eq. (10) with a constant Gaussian curvature $K = K_0 + \delta K \rightarrow K_0$. Since the shift from 3D to 2D ($\vec{\nabla} \rightarrow \vec{\nabla}_{xy}$) is a consequence of imposing the Killing vector n^μ on the metric tensor $g_{\mu\nu}$ in 3D + 1 dimensions, we first solve the eq. (10) in 3D to yield, $g_{00} = 1 - \ln K_0|\vec{x} - \vec{x}_0|^2 = 1 - 2\Phi$ with $\vec{x} = (x, y, z)$ and $\vec{x}_0 = (x_0, y_0, z_0)$, then restrict the solution to the $x - y$ plane by setting $z = z_0$.

This solution can be plugged into eq. (2b) to yield $2\pi\chi = \int_M K(r)d(Area) = -\pi\ln(K_0r^2)|_M = -2\pi\chi\ln(K_0r^2)^{2/\chi}|_M$ which requires that $(K_0r^2)^{2/\chi} \rightarrow \exp(-1) = \lim_{\chi/2\rightarrow 0}(1-\chi/2)^{2/\chi}$ to satisfy the Gauss-Bonnet theorem. Thus, this approximation suggests that perturbing K_0 around the ground state, $\chi/2 = 1 - g \rightarrow 0$ of the system leads to $K_0r_M^2 \rightarrow 1 - \chi/2 = g$ which is an expression of area quantisation, $\mathcal{A}_M(g) \propto r_M^2 = gK_0$, of the surface where in our case we can freely choose $\mathcal{A}_M(g = 1, 2, 3, \cdots)$ to be the unit area of the quasi-stable configurations with $g = 1, 2, 3\cdots$ vacancies as depicted in **Figure 2(d), (e)** & **(f)**.

Quasi-stable configurations as the analogues of Tori in 2D We shall name each configuration *a (3) three-(leaf) clover* where each honeycomb area is taken as a single leaf in the clover. Consequently, each vacancy g lies within a 3-leaf clover at the leaf stalk. We label each cation in the

honeycomb lattice as a *vertex* V, the line connecting to their adjacent neighbour as an *edge* E and each honeycomb unit *area* as A. Our theory then requires the number of honeycomb unit *areas* to be left unchanged by the extraction process.[n] Thus, for a honeycomb lattice with no vacancies, $A = F$ and $\chi = A - E + V = 2$. On the other hand, introducing $-g$ vacancies (equivalent to extracting g cations from the honeycomb surface) each at the stalk of the 3-leaf configuration, we find $A \to A$, $E \to E+3g$ and $V \to V+g$. Thus, the Euler characteristic defined above transforms to $\chi \to \chi' = A - (E + g) + (V + g) = (A - E + V) - 2g = 2 - 2g$ as expected.

5 Discussion

We are left to puzzle the question of why a geometric (gravitational) theory arises in the crystal and its explicit relation to the honeycomb. We note that the 3D crystal is considered electrochemically neutral when the 2D honeycomb structure bears no vacancies in the lattice. However, its intrinsic Gaussian curvature given by 2Λ is not guaranteed to vanish. Since adiabatic variations from this intrinsic curvature can occur by extraction of cations from the honeycomb surface leading to vacancies which we identify as the genus of the surface, this links the curvature variations to changes in the number density of the extracted cations. In essence, this is the origin of the geometric (gravitational) description. Hence, the physics of these curvature deformations which affect the transport properties of the cations are captured by an emergent field Φ that has a gravitational description.

Moreover, the extracted cations contribute to a diffusion current density via an adiabatic (weak field limit) Chern-Simons term that naturally arises in 2D electrodynamics. In addition, non-

[n] The number of honeycomb *faces* F does not remain unchanged.

adiabatic extractions ought to lead to the propagation of stress, energy and momentum through the crystal as sound waves, analogous to gravitational waves in general relativity. Quantum mechanically, the sound waves act as phonons that offer a mechanism to mediate an attractive force between the cations leading to the Cooper-pair problem and the onset of superconductivity.[58,59] Finally, we believe that the heuristic model proposed herein offers a glimpse of the relationship between geometry, quantum mechanics and thermodynamics perhaps useful in formulating a quantum theory of gravity.

1. Masese, T. et al. Rechargeable potassium-ion batteries with honeycomb-layered tellurates as high voltage cathodes and fast potassium-ion conductors. *Nat. Commun.* **9**, 3823 (2018).

2. Sathiya, M. et al. $\mathrm{Li_4NiTeO_6}$ as a positive electrode for Li-ion batteries. *Chem. Commun.* **49**, 11376-11378 (2013).

3. Yang, Z.et al. A high-voltage honeycomb-layered $\mathrm{Na_4NiTeO_6}$ as cathode material for Na-ion batteries. *J. Power Sources* **360**, 319-323 (2017).

4. Yuan, D. et al. A Honeycomb-Layered $\mathrm{Na_3Ni_3SbO_6}$: A High-Rate and Cycle-Stable Cathode for Sodium-Ion Batteries. *Adv. Mater.* **26**, 6301-6306 (2014).

5. Gupta, A., Buddie Mullins, C. & Goodenough, J. B. $\mathrm{Na_2Ni_2TeO_6}$: Evaluation as a cathode for sodium battery. *J. Power Sources* **243**, 817-821 (2013).

6. Masese, T et al. A high voltage honeycomb layered cathode framework for rechargeable potassium-ion battery: P2-type $\mathrm{K_{2/3}Ni_{1/3}Co_{1/3}Te_{1/3}O_2}$. *Chem. Commun.* **55**, 985-988 (2019).

7. Masese, T et al. Sulfonylamide-Based Ionic Liquids for High-Voltage Potassium-Ion Batteries with Honeycomb Layered Cathode Oxides. *ChemElectroChem* **6**, 3901-3910 (2019).

8. Evstigneeva, M. A., Nalbandyan, V. B., Petrenko, A. A., Medvedev, B. S. & Kataev, A. A. A new family of fast sodium ion conductors: $\mathrm{Na_2M_2TeO_6\ (M = Ni, Co, Zn, Mg)}$. *Chem. Mater.* **23**, 1174-1181 (2011).

9. Zheng, L. & Obrovac, M. N. Honeycomb Compound $\mathrm{Na_3Ni_2BiO_6}$ as Positive Electrode Material in Na Cells. *J. Electrochem. Soc.* **163**, A2362-A2367 (2016).

10. Ma, J. et al. Ordered and Disordered Polymorphs of $NaNi_{2/3}Sb_{1/3}O_2$: Honeycomb-Ordered Cathodes for Na-Ion Batteries. *Chem. Mater.* **27**, 2387-2399 (2015).

11. Nalbandyan, V. B., Petrenko, A. A. & Evstigneeva, M. A. Heterovalent substitutions in $Na_2Ni_2TeO_6$ family: Honeycomb-Ordered Cathodes for Na-Ion Batteries Crystal structure, fast sodium ion conduction and phase transition of $Na_2LiFeTeO_6$. *Solid State Ionics* **233**, 7-11 (2013).

12. Li, Y. et al. A P2-Type Layered Superionic Conductor Ga-Doped $Na_2Zn_2TeO_6$ for All-Solid-State Sodium-Ion Batteries. *Chem. - A Eur. J.* **24**, 1057-1061 (2018).

13. Li, Y. et al. New P2-Type Honeycomb-Layered Sodium-Ion Conductor: $Na_2Mg_2TeO_6$. *ACS Appl. Mater. Interfaces* **10**, 15760-15766 (2018).

14. Wu, J.-F., Wang, Q. & Guo, X. Sodium-ion conduction in $Na_2Zn_2TeO_6$ solid electrolytes. *J. Power Sources* **402**, 513-518 (2018).

15. Deng, Z et al. Ca-doped $Na_2Zn_2TeO_6$ layered sodium conductor for all-solid-state sodium-ion batteries solid electrolytes. *Electrochim. Acta* **298**, 121-126 (2019).

16. Dubey, M et al. Structural and ion transport properties of sodium ion conducting $Na_2M_2TeO_6$ (M = MgNi and MgZn) solid electrolytes. *Ceram. Int.* **298**, 121-126 (2019).

17. Kumar, V., Bhardwaj, N., Tomar, N., Thakral, V. & Uma, S. Novel lithium-containing honeycomb structures. *Inorg. Chem.* **51**, 10471–10473 (2012).

18. Zvereva, E. A. et al. A new layered triangular antiferromagnet Li_4FeSbO_6: Spin order, field-induced transitions and anomalous critical behavior. *Dalton Trans.* **42**, 1550–1566 (2013).

19. Derakhshan, S., Cuthbert, H. L., Greedan, J. E., Rahaman, B. & Saha-Dasgupta, T. Electronic structures and low-dimensional magnetic properties of the ordered rocksalt oxides $Na_3Cu_2SbO_6$ and $Na_2Cu_2TeO_6$. *Phys. Rev. B - Condens. Matter Mater. Phys.* **76**, 1–7 (2007).

20. Viciu, L. et al.Structure and basic magnetic properties of the honeycomb lattice compounds $Na_2Co_2TeO_6$ and $Na_3Co_2SbO_6$. *J. Solid State Chem.* **180**, 1060–1067 (2007).

21. Morimoto, K., Itoh, Y., Michioka, C., Kato, M. & Yoshimura, K. Magnetic excitation and Na-deficient effects on spin-gapped compound. *J. Magn. Magn. Mater.* **310**, 1254–1256 (2007).

22. Derakhshan, S., Greedan, J. E., Katsumata, T. & Cranswick, L. M. D. Long-Range Antiferromagnetic Ordering in the Novel Magnetically Frustrated Rock Salt Oxide System: $Li_3Mg_2RuO_6$. *Chem. Mater.* **20**, 5714–5720 (2008).

23. Zvereva, E. A. et al. Monoclinic honeycomb-layered compound $Li_3Ni_2SbO_6$: Preparation, crystal structure and magnetic properties. *Dalton Trans.* **41**, 572–580 (2012).

24. Upadhyay, S. K., Iyer, K. K., Rayaprol, S., Paulose, P. L. & Sampathkumaran, E. V. A rock-salt-type Li-based oxide, $Li_3Ni_2RuO_6$, exhibiting a chaotic ferrimagnetism with cluster spin-glass dynamics and thermally frozen charge carriers. *Sci. Rep.* **6**, 31883 (2016).

25. Koo, C. et al. Static and Dynamic Magnetic Response of Fragmented Haldane-like Spin Chains in Layered $Li_3Cu_2SbO_6$. *J. Phys. Soc. Jpn.* **85**, 084702 (2016).

26. Zvereva, E. A. et al. Orbitally induced hierarchy of exchange interactions in the zigzag antiferromagnetic state of honeycomb silver delafossite $Ag_3Co_2SbO_6$. *Dalton Trans.* **45**, 7373–7384 (2016).

27. Zvereva, E. A., Stratan, M. I., Shukaev, I. L., Nalbandyan, V. B. & Vasil'ev, A. N. Effect of a structural disorder on the magnetic properties of the sodium–cobalt tellurate $Na_{3.70}Co_{1.15}TeO_6$. *J. Exp. Theor. Phys.* **124**, 612–616 (2017).

28. Kumar, V., Gupta, A. & Uma, S. Formation of honeycomb ordered monoclinic $Li_2M_2TeO_6(M = Cu, Ni)$ and disordered orthorhombic $Li_2Ni_2TeO_6$ oxides. *Dalton Trans.* **42**, 14992 (2013).

29. Berthelot, R. et al. New layered compounds with honeycomb ordering: $Li_3Ni_2BiO_6$, $Li_3NiM'BiO_6$ $(M' = Mg, Cu, Zn)$, and the delafossite $Ag_3Ni_2BiO_6$. *Inorg. Chem.* **51**, 5377–5385 (2012).

30. Laha, S. et al. New rock salt-related oxides $Li_3M_2RuO_6$ $(M = Co, Ni)$: Synthesis, structure, magnetism and electrochemistry. *J. Solid State Chem.* **203**, 160–165 (2013).

31. Taylor, Z. N. et al. Stabilization of O–O Bonds by d0 Cations in $Li_{4+x}Ni_{1-x}WO_6$ $(0 \leq x \leq 0.25)$ Rock Salt Oxides as the Origin of Large Voltage Hysteresis. *J. Am. Chem. Soc.* **141**, 7333–7346 (2019).

32. Roudebush, J. H. et al. Structure and Magnetic Properties of $Cu_3Ni_2SbO_6$ and $Cu_3Co_2SbO_6$ Delafossites with Honeycomb Lattices. *Inorg. Chem.* **52**, 6083–6095 (2013).

33. Uma, S. & Gupta, A. Synthesis and characterization of new rocksalt superstructure type layered oxides $Li_{4.5}M_{0.5}TeO_6(M(III) = Cr, Mn, Al, Ga)$. *Mater. Res. Bull.* **76**, 118–123 (2016).

34. He, Z., Guo, W., Cui, M. & Tang, Y. Synthesis and magnetic properties of new tellurate compounds $Na_4MTeO_6(M = Co$ and $Ni)$ with a ferromagnetic spin-chain structure. *Dalton Trans.* **46**, 5076–5081 (2017).

35. He, Z., Cui, M. & Qiu, C. Synthesis, structure and magnetic behaviors of a new spin-1/2 chain compound Na_4CuTeO_6. *J. Alloys Compd.* **748**, 794–797 (2018).

36. Schmidt, W., Berthelot, R., Sleight, A. W. & Subramanian, M. A. Solid solution studies of layered honeycomb-ordered phases O_3-$Na_3M_2SbO_6(M = Cu, Mg, Ni, Zn)$. *J. Solid State Chem.* **201**, 178–185 (2013).

37. Heymann, G. et al. $Li_3Co_{1.06}TeO_6$: synthesis, single-crystal structure and physical properties of a new tellurate compound with Co^{II}/Co^{III} mixed valence and orthogonally oriented Li-ion channels. *Dalton Trans.* **46**, 12663–12674 (2017).

38. Bette, S. et al. Crystal structure and stacking faults in the layered honeycomb, delafossite-type materials $Ag_3LiIr_2O_6$ and $Ag_3LiRu_2O_6$. *Dalton Trans.* **48**, 9250–9259 (2019).

39. Grundish, N. S., Seymour, I. D., Henkelman, G. & Goodenough J. B. Electrochemical Properties of Three $Li_2Ni_2TeO_6$ Structural Polymorphs. *Chem. Mater.* **31**, 9379-9388 (2019).

40. Bhardwaj, N., Gupta, A. & Uma, S. Evidence of cationic mixing and ordering in the honeycomb layer of $Li_4M_2SbO_6$ (M(iii) = Cr, Mn, Al, Ga) (S.G. C2/c) oxides. *Dalton Trans.* **43**, 12050–12057 (2014).

41. Chern, S.-S. & Simons, J. Characteristic forms and geometric invariants. *Ann. Math.* **99** No. 1, 48–69 (1974).

42. Dunne, G. V. Aspects of Chern-Simons Theory. arXiv hep-th/9902115 (1999).

43. Chavel, I. Riemannian Geometry: A Modern Introduction. *New York: Cambridge University Press*, (1994).

44. Allendoerfer, C. B. & Weil, A. The Gauss-Bonnet Theorem for Riemannian Polyhedra. *Trans. Amer. Math. Soc.* **53**, 101–129 (1943).

45. Feynman, R. P. Feynman's Thesis — A New Approach to Quantum Theory. *World Scientific* (2005).

46. Zee, A.Quantum Field Theory in a Nutshell. *Princeton University Press , Princeton and Oxford* (2010)

47. Wagner, M. Unitary Transformations in Solid State. *Elsevier Science* (1986).

48. Aharonov, Y. & Casher, A.Topological Quantum Effects for Neutral Particles.*Phys. Rev. Lett.* **53** 319 (1984).

49. Kanyolo, G. M. Berry's Phase and Renormalization of Applied Oscillating Electric Fields by Topological Quasi-Particles. *arXiv* 1909.00778 (2019).

50. Risken, H. The Fokker-Planck Equation: Methods of Solution, Applications. *Springer-Verlag, Berlin, New York* 1996.

51. Kanyolo, G. M. & Shimada H.Lifting of Coulomb Blockade by Alternating Voltages in Small Josephson Junctions with Electromagnetic Environment-Based Renormalization Effects. *arXiv* 1911.10899 (2019)

52. Bialynicki-Birula, I. & Bialynicka-Birula, Z.The role of the Riemann–Silberstein vector in classical and quantum theories of electromagnetism *IOP Publishing Ltd Journal of Physics A: Mathematical and Theoretical* **46** No. 5 (2013).

53. Fryberger, D. On generalized electromagnetism and Dirac algebra. *Found. Phys.* **19** 125–159 (1989).

54. Verlinde, E. On the origin of gravity and the laws of Newton. *J. High Energ. Phys.* **29** (2011).

55. Misner, C. W., Thorne K. S.& Wheeler, J.A.Gravitation. *New York: W.H. Freeman and Company* (1973).

56. Carroll, S. Spacetime and Geometry: An Introduction to General Relativity. *Addison-Wesley* (2003).

57. Carroll, S. Lecture Notes on General Relativity. *arXiv* gr-qc/9712019 (1997).

58. Cooper, Leon N. Bound electron pairs in a degenerate Fermi gas. *Phys. Rev.* **104**, 1189–1190 (1956).

59. Bardeen, J. Electron-Phonon Interactions and Superconductivity. In: Haken H., Wagner M. (eds) Cooperative Phenomena.*Springer, Berlin, Heidelberg* 63-78 (1973).

Acknowledgements Part of this work was conducted under the auspices of the National Institute of Advanced Industrial Science Technology (AIST), Japan Society for the Promotion of Science (JSPS KAKENHI Grant Numbers 19 K15685) and Japan Prize Foundation.

Competing Interests The authors declare that they have no competing financial interests.

Correspondence Correspondence and requests for materials should be addressed to Titus Masese (Email: titus.masese@aist.go.jp) and requests for clarification of aspects related to the model to Godwill Mbiti Kanyolo (Email: gmkanyolo@gmail.com)

Appendix

A Inter-distance Tuning

The possibility of tuning the distance between the honeycomb layers (viz., interslab / inter-layer distance) with the introduction of A cations with larger ionic radii, avails avenues to tune the inter-layer magnetic couplings; hence the feasibility to adjust the dimensionality of the magnetic lattice. Honeycomb layered compositions of $\mathrm{A_2^+L_2^{2+}Te^{6+}O_6}$ ($\mathrm{A_{2/3}^+L_{2/3}^{2+}Te_{1/3}^{6+}O_2}$) had initially been relegated to $\mathrm{A = Li, Na}$; however, recent reports have shown that such compositions can be extended to lithophile large-atoms such as K.[1] This is an additional advantage as these series of honeycomb compositions may be expanded to new compositions where $\mathrm{A = Rb^+, Cs^+, Ag^+, Au^+, Cu^+, H^+}$, and so forth. A correlation exists between the ionic radii of A and the inter-layer distance (z), as explicitly shown in inset of **Figure 1**. Moving from $\mathrm{Li, Na}$ to K, it is clear that there is a propensity of the inter-layer distance to increase; which consequently should affect the transport properties (id

est, diffusion nature of alkali A atoms) along the two-dimensional (2D) surface. **Figure 1** (inset, right) depicts the nature of motion of K^+ in $K_{2/3}Ni_{1/3}Te_{1/3}O_2$ $(K_2Ni_2TeO_6)$,[1] which is greatly influenced by the arrangement of NiO_6 and TeO_6 octahedra that reside in the slabs.

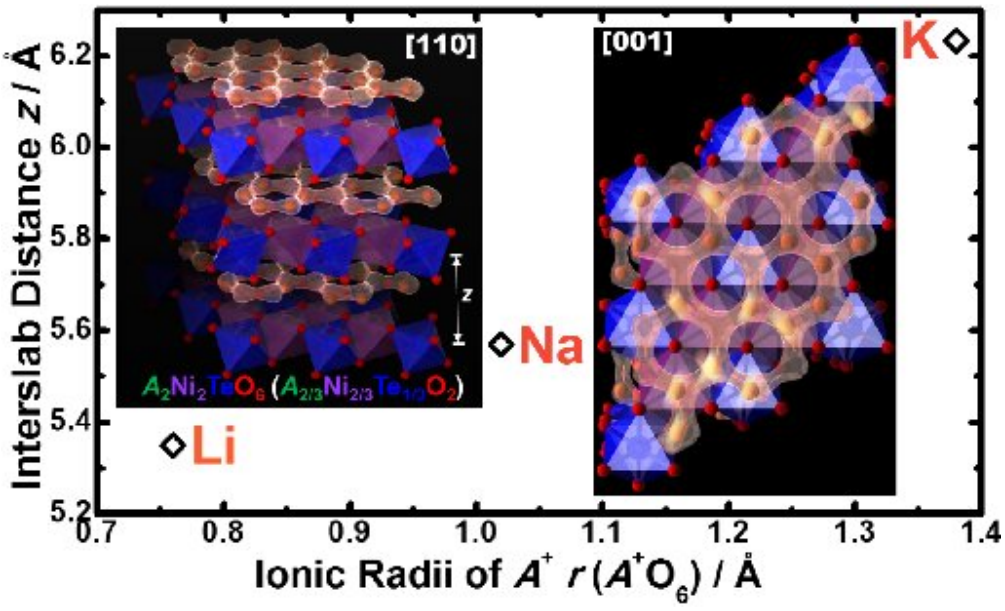

Figure 1: Trend in increase of the interslab/inter-layer distance (z) for honeycomb layered oxides, adopting the composition $\mathrm{A}_2^{+}\mathrm{Ni}_2^{+2}\mathrm{Te}^{6+}\mathrm{O}_6$ ($\mathrm{A}^{+}_{2/3}\mathrm{Ni}^{2+}_{2/3}\mathrm{Te}^{6+}_{1/3}\mathrm{O}_2$), with increase in ionic radius of A cations. Inset (left) shows a polyhedral view of the layered structure of $\mathrm{A}_2\mathrm{Ni}_2\mathrm{TeO}_6$ along the z-axis: Ni octahedra are shown in purple, Te octahedra are in blue, while A ions are brown spheres and O ions are small red spheres. Inset (right) depicts a fragment of the honeycomb structure along the $x-y$ plane with a two-dimensional (2D) motion of A ions that reside above or below the honeycomb slabs.

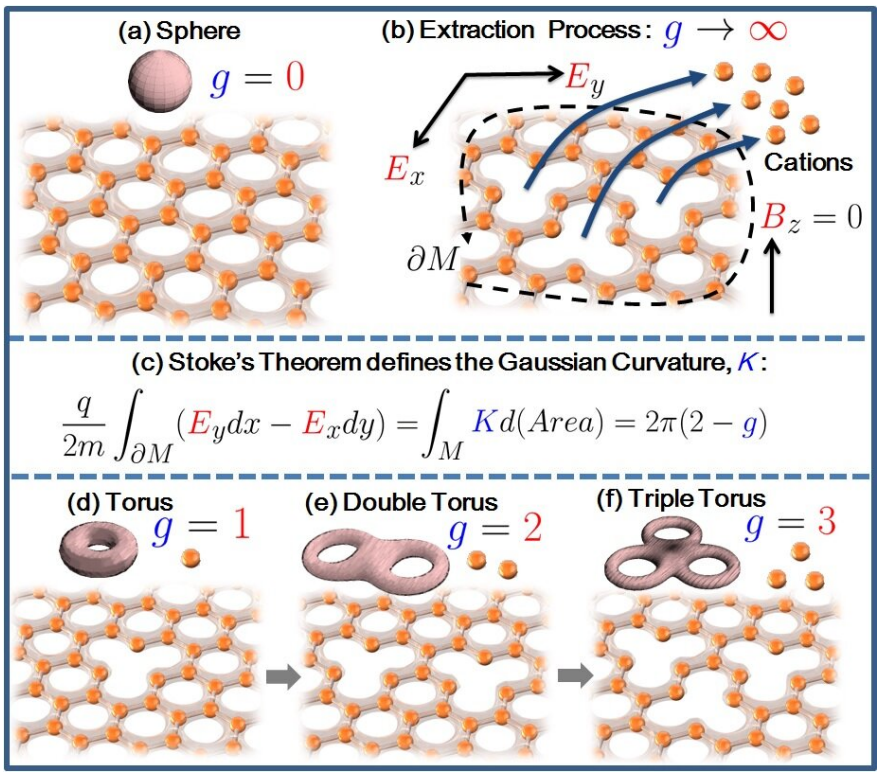

Figure 2: Various quasi-stable configurations of the cation honeycomb layers and the directions of the electric and magnetic field. (a) The cations arranged in a honeycomb fashion with no cationic vacancies ($g = 0$) topologically equivalent to the sphere. (b) The extraction process of $g \to \infty$ cations from the honeycomb surface by applied electric fields E_x and E_y. The magnetic field in the $B_z = 0$ is taken to be zero. Vacancies created by this extraction process can be counted by tracking the change in the electric fields at the boundary of the honeycomb surface ∂M. (c) The equation that tracks the changes where m and q are the mass and charge of a single cation and K the Gaussian curvature of the surface. Applying Stokes's theorem transforms the equation to the Gauss-Bonnet theorem where g is the genus. (d) The honeycomb surface with vacancy $g = 1$ equivalent to a torus. (e) The honeycomb surface with vacancy $g = 2$ equivalent to a double torus. (f) The honeycomb surface with vacancy $g = 3$ equivalent to a triple torus.